



# An adaptive fast multipole boundary face method with higher order elements for acoustic problems in three-dimension

Xianhui Wang, Jianming Zhang\*, Fenglin Zhou, Xingshuai Zheng

State Key Laboratory of Advanced Design and Manufacturing for Vehicle Body, College of Mechanical and Vehicle Engineering, Hunan University, Changsha 410082, China

## ARTICLE INFO

### Article history:

Received 10 July 2012

Accepted 7 September 2012

### Keywords:

Fast multipole boundary face method  
Burton-Miller equation  
Acoustic wave problems  
Adaptive tree data structure  
High order elements

## ABSTRACT

An adaptive fast multipole boundary face method using higher order elements based on the well-known Burton-Miller equation is presented in this paper for solving the large-scale three-dimensional exterior acoustic wave problems. The fast multipole boundary face method is referred to as FMBFM. In the FMBFM, the boundary integration and field variables approximation are both performed in the parametric space of each boundary face exactly the same as the B-rep data structure in standard solid modeling packages. In this FMBFM, higher order elements are employed to improve the computational accuracy and efficiency, and an adaptive tree structure is constructed to improve the efficiency of the FMBFM. Numerical examples for large-scale acoustic radiation and scattering problems in this paper demonstrated the accuracy, efficiency and validity of the adaptive FMBFM. Comparison study showed that the FMBFM with high order elements out-performs the FMBFM with constant elements respect to accuracy and CPU time at the same number of the nodes. In addition, the CAD models, even with complicated geometry, are directly converted into the FMBFM models, thus the present method provides a new way toward automatic simulation.

© 2012 Elsevier Ltd. All rights reserved.

## 1. Introduction

The boundary face method (BFM) [1] based on the boundary integral equation (BIE) is a numerical approach for solving field problems. Several works have been published to improve or extend the applicability of the BFM. Qin and Zhang [2] implemented the BFM using finite elements defined in the parametric space of boundary faces, which can be considered as a new implementation of the boundary element method (BEM). Gu and Zhang [3] applied the BFM to solve linear elasticity problems using B-spline element interpolation. In [4], Zhou et al. combined the dual reciprocity method (DRM) and the BFM to solve non-homogeneous potential problems. Other applications of BFM can be found in [5–7]. However, few works have been done for acoustic problems in the BFM.

In [8–13], the conventional BEM was applied for acoustic exterior problems. Chen et al. [8] employed the combined Helmholtz integral equation formulation (CHIEF) to study the acoustic exterior problem in conjunction with the singular value decomposition (SVD). They propose some suggestions for selecting those interior points were recommended in the paper. If properly chosen, only two interior points may be needed.

The CHIEF is proposed by Schenck [9]. In that method, some additional Helmholtz integral relations were added in the interior domain. This additional relation leads to an over-determined system of equations, which can be solved using a least-squares technique. In the conventional BEM, the error mainly comes from two aspects. One is the computational error, and the other one is the discretization error which contains the geometries error. However, the BFM circumvent the geometries error in the computation. In BFM, both boundary integration and interpolation of field variables are performed in the parametric space of each boundary face. The geometric data at Gaussian integration points, such as the coordinates, the Jacobians and the out normals are calculated directly from the faces rather than from element interpolation. Thus the geometric errors are avoided. And as in the BEM, only the boundary discretization is required in the BFM, which implies a very low cost for mesh generation and preprocessing [9,10]. For acoustic exterior problems, the radiation condition at infinity can be satisfied automatically. Despite above these advantages, however, in the BFM, the system matrix is dense and unsymmetrical, requiring  $O(N^2)$  memory and  $O(N^3)$  operations with  $N$  being the number of nodes, when the direct solvers are used. As a result, the BFM is prohibitively expensive when it is used to solve large-scale problems. Due to the memory limitation of the computer resource, the number of the nodes in our BFM program that could be analyzed only is no more than 3000. To circumvent this problem, this paper presents an adaptive

\* Corresponding author. Tel.: +86 731 88823 061.

E-mail address: zhangjianm@gmail.com (J. Zhang).

fast multipole boundary face method (FMBFM) based on a weakly singular integral forms' Burton-Miller equation [10] for 3-D radiation and scattering of acoustic problems. The weakly singular integral forms' of the Burton-Miller equation is presented by Liu [11]. And the boundary face method with Burton-Miller equation is referred to as CHBFM in this paper. In the adaptive FMBFM, the analytical integrations cannot be performed, thus we employed higher order elements to improve the accuracy and efficiency. The FMBFM has been integrated into the widely used commercial CAD package UG-NX, and thus able to handle problems with complicated geometries. A tree data structure with tight bounds, which is constructed by binary tree, is used to hierarchically subdivide the computational domain into well-separated cells and to invoke the multipole expansion approximation. This adaptive tree structure is proposed by Zhang [14,15] based on Anderson's work [16]. In the adaptive tree, rectangular boxes is used to instead of cubes, the boxes are subdivided according to the shapes of the computational models. Therefore the adaptive tree is more flexible in matching the geometry of the computational domain. In addition, a more generalized Downward Pass algorithm is designed to allow M2L among the child boxes of a single parent box. The authors have demonstrated that the adaptive tree structure together with an adaptive selection of the expansion order is validity and could evidently improve the computational efficiency, especially for the slender structure.

To the boundary integral equation (BIE) method, many researchers have been devoted to improving the overall solution efficiency for systems of equations. Various techniques have been proposed to solve the large-scale problems, such as iterative solvers, parallel computing or sub-domain techniques. To accelerate the matrix-vector multiplication, the fast multipole method (FMM), which is regarded as one of the top 10 algorithms of the 20th century, was proposed by Rokhlin and Greengard [17,18]. The FMM in Rokhlin [17] was introduced as a fast solution method for integral equations for two dimensional Laplace's equation, the multipole moments associated with a distant group can be translated into the coefficients of the local expansion associated with a local group. And then Greengard [18] developed the FMM as an algorithm for the rapid evaluation of potential and force fields in a large scale ensemble of charged particles. In addition to Rokhlin's work, Greengard introduced a hierarchical decomposition of the domain geometry with a quad-tree in two dimensions and an oct-tree in three dimensions to carry out efficient and systematic grouping of particles. Employing the FMM for the matrix-vector multiplications in iterative solvers, the computing cost can be reduced from  $O(N^2)$  to  $O(N)$ . And there are two main solvers for the FMM, one is the generalized minimum residual (GMRES) method [19], the other is the conjugate gradient squared (CGS) method [20]. When the iterative solvers is used, the operation counts for the BFM is reduced from  $O(N^3)$  to  $O(N^2)$ . Consequently, the total number of operation counts for the fast multipole boundary element method (FMBEM) or FMBFM with iterative solvers is reduce from  $O(N^3)$  to  $O(N)$ . And also the memory requirement reduced to  $O(N)$ . Therefore the large-scale computations can be promised. The FMM has been applied to elastostatic problems [21], crack problems [22], Helmholtz problems [23], and incorporation with hybrid boundary node method by Zhang [24]. A new version of the FMM for Laplace problem was proposed by Greengard and Rokhlin [25], which can huge improve the efficiency of the FMM. Many other research works have been published to improve and extend the applicability of the FMM [26–28].

The FMM has been applied to acoustic problems since 1990s. A diagonal form FMM for Helmholtz equation was proposed by Rokhlin [23]. Since then, lots of works have been made by many researchers [29–37]. Chen et al. [29] employed the FMM to

accelerate the construction of influence matrix in the dual boundary element methods (DBEM). This separable technique promotes the efficiency in determining the influence coefficients. Epton and Dembart [30] presented a concise summary of multipole translations for 3-D Helmholtz equations. A more precise error estimates introduced for the FMM was provided by Darve [31]. A recurrence relations is developed by Chew [32], then was extended by Gumerov and Duraiswami [33] to develop a general recursive method for obtaining the translation matrices. The method can provide a huge improvement in the efficiency of the FMM. Shen [34] proposed an adaptive FMM for 3-D full space acoustic problems. The adaptive FMM algorithm can be several times faster than the non-adaptive one. Bapat [35] applied the adaptive FMM for 3-D half space acoustic problems. Using the half-space Green's function, only the local expansion is different from that for 3-D full-space FMM. The total CPU time and memory storage are also reduced by about a half for large scale half-space acoustic problems. Analytic integration of the moments in the diagonal form FMM for 3-D acoustic problems was proposed by Wu [36].

The paper is organized as follows: Section 2 mainly reviews the BIEs and the BFM for the acoustic wave problems. In Section 3, the multipole expansion formulations are described followed by the adaptive tree structure in Section 4. In Section 5, several numerical examples are given to demonstrate the accuracy, efficiency and validity of the present FMBFM. The paper ends with conclusions and discussions on future work in Section 6.

## 2. Review of the BIE formulations and the BFM

### 2.1. BIE formulations for acoustic wave problems

In 2-D or 3-D spaces, the governing equation for acoustic wave problem is the Helmholtz equation which can be written as:

$$\nabla^2 \phi(x) + k^2 \phi(x) = 0, \quad x \in E, \quad (1)$$

in which  $x$  is the field point,  $E$  is the acoustic domain,  $\phi(x)$  denotes the total sound pressure at  $x$ ,  $\nabla^2$  denotes the Laplace operator,  $k = 2\pi f/c$  denotes the wave number,  $f$  is the cyclic frequency,  $c$  is the speed of sound in the acoustic medium.

The boundary conditions for the governing equation of acoustic wave problems can be described as:

$$\begin{cases} \text{Dirichlet type} & \phi = \bar{\phi}, & \forall x \in S \\ \text{Neumann type} & q = \frac{\partial \phi}{\partial n} = \bar{q} = ikc\rho v_n, & \forall x \in S, \\ \text{Impedance type} & \phi = Zv_n, & \forall x \in S \end{cases} \quad (2)$$

where  $c$  denotes the sound velocity in medium.  $\rho$  is the mass density.  $v_n$  is the normal velocity.  $n$  is the outward normal.  $Z$  denotes the specific acoustic impedance. The quantities with over bars indicate given values.  $i = \sqrt{-1}$ . For the exterior acoustic problem, the Sommerfeld radiation condition must be satisfied at infinite field. It is:

$$\lim_{R \rightarrow \infty} \left[ R \left[ \frac{\partial \phi}{\partial R} - ik\phi \right] \right] = 0, \quad (3)$$

where  $R$  is the distance from a fixed origin to a general field point.  $\phi$  is the radiated wave in a radiation problem or the scattered wave in a scattering problem.

The integral representation of the solution to the Helmholtz equation is:

$$\begin{aligned} c(P_0)\phi(P_0) = & \int_S G(P_0, P)q(P)dS(P) - \int_S \frac{\partial G(P_0, P)}{\partial n} \phi(P)dS(P) \\ & + \phi^I(P_0), \end{aligned} \quad (4)$$

here  $G(P_0, P) = \frac{e^{ikr}}{4\pi r}$  denotes the full space Green's function of Helmholtz problems, in which  $r = |P - P_0|$  is the distance between source point  $P_0$  and filed point  $P$ .  $q(P) = \frac{\partial \phi(P)}{\partial n}$ ,  $\phi^I(P_0)$  denotes a prescribed incident wave but it does not exist in radiation problems. Coefficient  $c(P_0)$  is described as:

$$c(P_0) = \begin{cases} 1 & P_0 \in E \\ \frac{1}{2} & P_0 \in S, \\ 0 & P_0 \in B \end{cases} \quad (5)$$

where  $E$  is the exterior region (acoustic medium).  $S$  denotes the boundary which is smooth around  $P_0$ .  $B$  is the interior region (a body or scatterer).

To derive the hyper-singular BIE (HBIE), we take the derivative of Eq. (4) with respect to the outward normal  $n_0$  at source point  $P_0$ . The following boundary integral equation is given:

$$c(P_0) \frac{\partial \phi(P_0)}{\partial n_0} = \int_S \frac{\partial G(P_0, P)}{\partial n_0} \frac{\partial \phi(P)}{\partial n} dS(P) - \int_S \frac{\partial^2 G(P_0, P)}{\partial n \partial n_0} \phi(P) dS(P) + \frac{\partial \phi^I(P_0)}{\partial n_0}, P_0 \in S, \quad (6)$$

here  $c(P_0)$  is 1/2 if  $S$  is smooth around of the source point  $P_0$ . Based on the Burton-Miller equation in Ref. [10], a complex linear combination (CHBIE) of the CBIE (4) and HBIE (6) is obtained to yield a unique solution for all the wave numbers:

$$\beta \left[ \int_S \frac{\partial^2 G(P_0, P)}{\partial n \partial n_0} \phi(P) dS(P) \right] + \int_S \frac{\partial G(P_0, P)}{\partial n} \phi(P) dS(P) + c(P_0) \phi(P_0) = \beta \left[ \int_S \frac{\partial G(P_0, P)}{\partial n_0} \frac{\partial \phi(P)}{\partial n} dS(P) - c(P_0) \frac{\partial \phi(P_0)}{\partial n_0} \right] + \int_S G(P_0, P) \frac{\partial \phi(P)}{\partial n} dS(P) + \beta \frac{\partial \phi^I(P_0)}{\partial n_0} + \phi^I(P_0) \forall P_0 \in S, \quad (7)$$

$\beta = i/k$  is used as the imaginary coupling parameter of the Burton-Miller's formulation [38],  $k$  is the wave number.

In the Burton-Miller equation (7), the major difficulty is that the BIE contains strong singular integral (integrand has a  $1/r^2$  singularity) and hyper-singular integral equation (integrand has a  $1/r^3$  singularity). Here a weakly singular integral form which proposed by Ref. [11] is adopted to overcome this difficulty. In this BIE, the singularity in the strong singular or hyper-singular integral is regularized using a one-term or two-term subtraction, respectively, thus we could calculate all the integrals directly.

### 2.2. The BFM for acoustic wave problems

As in the BEM, only the boundary discretization is required in the BFM for solving acoustic wave problems. One of the essential differences between BFM and BEM is that boundary elements are built in different spaces, namely, elements used in BFM are located in the two-dimensional parametric space of the bounding surface, while in the BEM elements are located in the three-dimensional physical space. In the BFM, the geometric data over the elements are calculated directly from the surfaces using the following map  $F$ :

$$f(x, y, z) = f(x(t_1, t_2), y(t_1, t_2), z(t_1, t_2)) = f(t_1, t_2) \quad x, y, z \in \Omega \quad t_1, t_2 \in \bar{\Omega}, \quad (8)$$

where  $f$  is the geometric map function of the parametric space to physical surface, and  $t_1, t_2$  are the parametric coordinates which are constrained to the interval  $[0, 1]$  mostly.  $\Omega$  is the physical space, and  $\bar{\Omega}$  is the parametric space corresponding to  $\Omega$ . Through the geometric map  $F$ , the outward normals at the locations on the boundary, the shape functions and its derivatives can be constructed

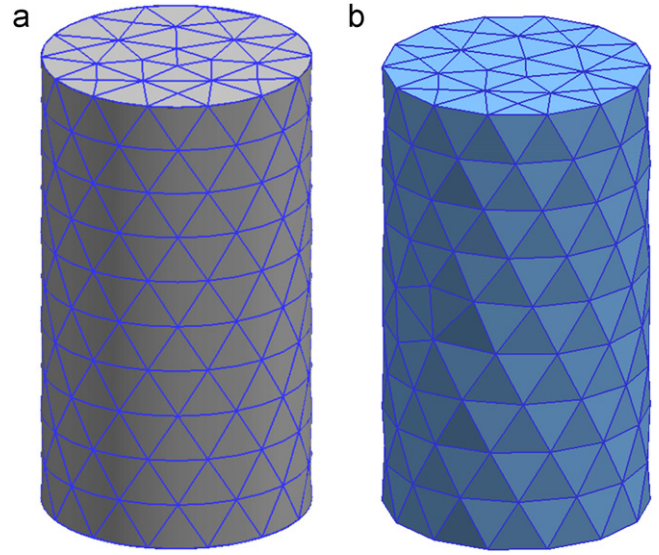


Fig. 1. Two types of boundary discretizations. (a) BFM elements, (b) BEM elements.

in the parametric space  $\bar{\Omega}$ . The detailed description and integration scheme can be found in Ref. [2].

To clearly show the differences of the discretization between the BFM and BEM, their boundary meshes on the same cylinder are shown in Fig. 1. The elements in BFM (Fig. 1(a)) keep exact geometry, while the elements in BEM (Fig. 1(b)) are used to approximate the geometry of the cylinder, thus introduces geometric errors. The geometric errors may lead to accuracy loss, which will be illustrated in the numerical examples in Section 4.

By dividing the boundary  $S$  into  $M$  elements and applying the shape functions on the element, we have the following approximations for variation of pressure and velocity:

$$\begin{aligned} \phi(P) &= \sum_{k=1}^{N^E} N_k(P) \phi_k = \sum_{k=1}^{N^E} N_k(t_1, t_2) \phi_k, \\ q(P) &= \sum_{k=1}^{N^E} N_k(P) q_k = \sum_{k=1}^{N^E} N_k(t_1, t_2) q_k, \end{aligned} \quad (9)$$

where  $\phi_k$  and  $q_k$  denote the value of  $\phi$  and  $q$  at the  $k$ th node, respectively.  $N_k(\cdot)$  is the shape function associated with the  $k$ th node.  $N^E$  is the number of node in the element.

The discretized form of Eq. (7) can be obtained as the following forms:

$$\sum_{j=1}^M \sum_{\alpha=1}^{N^E} h_{ij}^{\alpha} \phi_{\alpha} = \sum_{j=1}^M \sum_{\alpha=1}^{N^E} g_{ij}^{\alpha} q_{\alpha} + b_i, \quad \text{for node } i = 1, 2, \dots, N, \quad (10)$$

here  $b_i$  is from the incident wave for the scattering problems,  $N$  denotes the total number of nodes, and

$$\begin{cases} h_{ij}^{\alpha} \phi_{\alpha} = \left[ \beta \int_{S_j} \frac{\partial^2 G(P_i, P)}{\partial n(P) \partial n(P_i)} N_{\alpha}(P) dS(P) + \int_{S_j} \frac{\partial G(P_i, P)}{\partial n(P)} N_{\alpha}(P) dS(P) + \sigma(P_i, P_{\alpha}) c(P_i) \right] \phi_{\alpha} \\ g_{ij}^{\alpha} q_{\alpha} = \left[ \beta \int_{S_j} \frac{\partial G(P_i, P)}{\partial n(P_i)} N_{\alpha}(P) dS(P) + \int_{S_j} G(P_i, P) N_{\alpha}(P) dS(P) - \sigma(P_i, P_{\alpha}) \beta c(P_i) \right] q_{\alpha} \end{cases} \quad (11)$$

here the  $S_j$  denotes the element  $j$ , and if the  $\alpha$ th node in the element  $j$  coincide with the  $i$ th node,  $\sigma(P_i, P_{\alpha}) = 1$ ; else  $\sigma(P_i, P_{\alpha}) = 0$ .

### 3. Review of multipole expansion formulations

The formulations of the multipole expansion for acoustic problems are described in this section for 3-D case. More detailed description can be found in Ref. [39].

### 3.1. The multipole expansion formulations for Helmholtz

The fundamental solution  $G(x,y) = \frac{e^{ikr}}{4\pi r}$  for Helmholtz equation in 3-D can be expanded into the following series:

$$G(x,y) = \frac{ik}{4\pi} \sum_{n=0}^{\infty} (2n+1) \sum_{m=-n}^n O_n^m(k,x-y_c) \bar{I}_n^m(k,y-y_c), |y-y_c| < |x-y_c|, \quad (12)$$

In which,  $y_c$  is an expansion point near  $y$ , and the function  $I_n^m$  and  $O_n^m$  can be further described as:

$$I_n^m = j_n(k|x|) Y_n^m\left(\frac{x}{|x|}\right),$$

$$O_n^m = h_n^{(1)}(k|x|) Y_n^m\left(\frac{x}{|x|}\right), \quad (13)$$

where  $\bar{I}_n^m$  is the complex conjugate of  $I_n^m$ .  $h_n^{(1)}$  and  $j_n$  are the  $n$ th order spherical Hankel function of first kind and  $n$ th order spherical Bessel function, respectively.  $Y_n^m$  denotes the spherical harmonics function which can be wrote as:

$$Y_n^m(x) = \sqrt{\frac{(n+m)!}{(n-m)!}} P_n^m(\cos \theta) e^{im\phi}, \quad (14)$$

here the coordinates of  $x$  in a spherical coordinate system is  $(\rho, \theta, \phi)$ .  $P_n^m$  is the associated Legendre function which is defined as:

$$P_n^m(x) = (1-x^2)^{m/2} \frac{d^m}{dx^m} P_n(x), \quad (15)$$

where  $P_n$  is the Legendre function.

With applying expansion (12), we can evaluate the integral with kernel  $G(x, y)$  in Eq. (4) through the following equation:

$$\int_{S_c} G(x,y)q(y)dS(y) = \frac{ik}{4\pi} \sum_{n=0}^{\infty} (2n+1) \sum_{m=-n}^n O_n^m(k,x-y_c) M_{n,m}(k,y_c),$$

$$|y-y_c| < |x-y_c|, \quad (16)$$

where  $M_{n,m}(k,y_c)$  denotes the multipole moments centered at  $y_c$ , its form is:

$$M_{n,m}(k,y_c) = \int_{S_c} \bar{I}_n^m(k,y-y_c)q(y)dS(y) \quad (17)$$

### 3.2. Multipole conversion

When the multipole moments center shift from  $y_c$  to  $y_{c'}$ , which is called moment to moment (M2M) translation, the multipole moments are translated according to the following form:

$$M_{n,m}(k,y_{c'}) = \sum_{n'=0}^{\infty} (2n'+1) \sum_{m'=-n'}^{n'} \sum_{l=|n-n'|}^{n+n'} (-1)^{m'} \times W_{n,n',m,m',l} I_l^{m-m'}(k,y_c-y_{c'}) M_{n',-m'}(k,y_c) \quad (18)$$

where  $W_{n,n',m,m',l}$  is calculated by the following formula:

$$W_{n,n',m,m',l} = (2l+1) i^{n'-n+l} \begin{pmatrix} n & n' & l \\ 0 & 0 & 0 \end{pmatrix} \begin{pmatrix} n & n' & l \\ m & m' & -m-m' \end{pmatrix}, \quad (19)$$

and  $\begin{pmatrix} \bullet & \bullet & \bullet \\ \bullet & \bullet & \bullet \\ \bullet & \bullet & \bullet \end{pmatrix}$  denotes the Wigner 3j symbol.

The local expansion for the  $G(x, y)$  integral in Eq. (4) can be described as the following form:

$$\int_{S_c} G(x,y)q(y)dS(y) = \frac{ik}{4\pi} \sum_{n=0}^{\infty} (2n+1) \sum_{m=-n}^n L_{n,m}(k,y,x_L) \bar{I}_n^m(k,x-x_L), \quad (20)$$

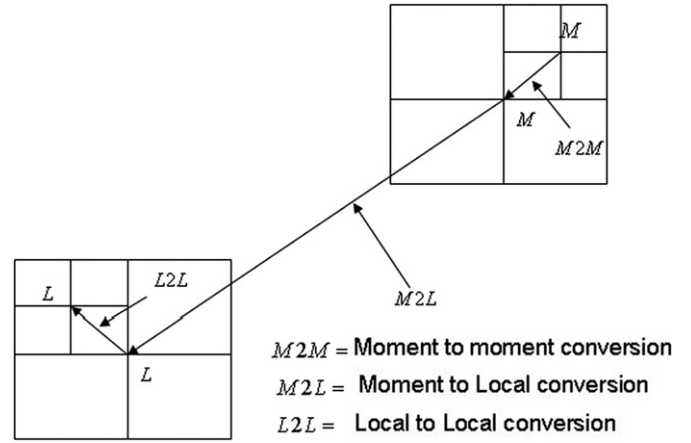


Fig. 2. Conversion of the FMM: M2M, M2L, L2L translations.

In the moment to local (M2L) translations, the local expansion coefficients are given by the following form:

$$L_{n,m}(k,y,x_L) = \sum_{n'=0}^{\infty} (2n'+1) \sum_{m'=-n'}^{n'} \sum_{l=|n-n'|}^{n+n'} \times W_{n',n,m',m,l} N_l^{m-m'}(k,x_L-y_c) M_{n',m'}(k,y_c), \quad (21)$$

for  $|x-x_L| < |y_c-x_L|$ , here  $x_L$  is the local expansion center and  $N_n^m$  is defined as:

$$N_n^m = h_n^{(1)}(k|x|) \bar{Y}_n^m\left(\frac{x}{|x|}\right), \quad (22)$$

If the local expansion center shift form  $x_L$  to  $x_{L'}$ , the form of the L2L translation is:

$$L_{n,m}(k,y,x_L) = \sum_{n'=0}^{\infty} (2n'+1) \sum_{m'=-n'}^{n'} \sum_{l=|n-n'|}^{n+n'} \times W_{n',n,m',-m,l} I_l^{m-m'}(k,x_L-x_{L'}) L_{n',m'}(k,y,x_{L'}), \quad (23)$$

M2M, M2L, L2L translations are illustrated in Fig. 2.

For computing the M2M, M2L and L2L translations of the integral with kernel  $\frac{\partial G(x,y)}{\partial n}$  Eq. (4), we replace  $M_{n,m}$  by  $H_{n,m}$  of which the expression is:

$$H_{n,m}(k,y_c) = \int_{S_c} \frac{\partial \bar{I}_n^m(k,y-y_c)}{\partial n} \phi(y) dS(y) \quad (24)$$

For calculating the integrals in Eq. (6), similar translation can be applied.

Finally, we substitute the above FMM formulations to Eq. (7), for the  $i$ th node  $x$ , and the  $\alpha$ th node which is in the  $j$ th element, the related term in Eq. (7) can be evaluated using the local expansion:

$$h_{ij}^{\alpha} \phi_{\alpha} \quad \text{or} \quad g_{ij}^{\alpha} q_{\alpha} = \frac{ik}{4\pi} \sum_{n=0}^{\infty} (2n+1) \sum_{m=-n}^n L_n^m(k,y_{\alpha},x_L) \left[ \bar{I}_n^m(k,x_L) + \beta \frac{\partial \bar{I}_n^m(k,x_L)}{\partial n_0} \right], \quad (25)$$

here  $x$  is far away from any point in element  $j$ . To calculate the integral over the elements which are near the field point  $x$ , the conventional Gaussian numerical integration method is applied in this paper.

#### 4. The adaptive tree structure

In the FMM analysis for acoustic problems, a tree structure is required to divide the geometry and to evaluate the integral. The standard FMM algorithm uses an oct-tree. The oct-tree is constructed by dividing the root cube enclosing the computational domain boundary into smaller and smaller sub-boxes until the number of elements in each sub-box is less than a given number. However, the tree structure in our research is an adaptive tree with tight bounds which is constructed by binary tree. In the FMM, the computational cost mainly depends on the M2L translation. So one efficient way to improve the efficiency is reducing the number of the M2L translations. In this paper, the FMM reduce the number of the M2L translations by decreasing the depth of the adaptive tree. In this process, an element is considered to be inside a box if the center of the element locates inside the box. The adaptive tree structure in the FMBFM with higher order elements can be described as follows:

Step 1: Initialization. A smallest box, which can contain the domain of the entire computational model, is constructed by searching the max and min values of  $x$ ,  $y$ ,  $z$  components of the coordinates among all the element centers. This box is the root box for constructing the tree structure.

Step 2: Constructing tree structure. The root box is subdivided into approximately cubic boxes at level 1, and these boxes are then subdivided into approximately cubes in the following subdivided. Stop dividing one box until the number of elements in the box is less than a given number.

Step 3: Searching for the adjacent cells and interaction cells of each cell.

After the above operation, an adaptive binary tree is constructed. This tree structure is based on the standard oct-tree structure, but differs in the following aspects:

1. The rectangular boxes are used instead of cubes. It is believed that a rectangular box is more flexible in matching structure.
2. A box in adaptive tree is split into child boxes based on its shape as showing in Fig. 3. For each subdividing, the longest side is considered and dividing first, and so on. Stop dividing until the ending rule act.
3. The boxes are tightened at each subdivision step. In adaptive tree, a smallest box, which is the tightened box, is used to enclose the cluster of the boundary elements.

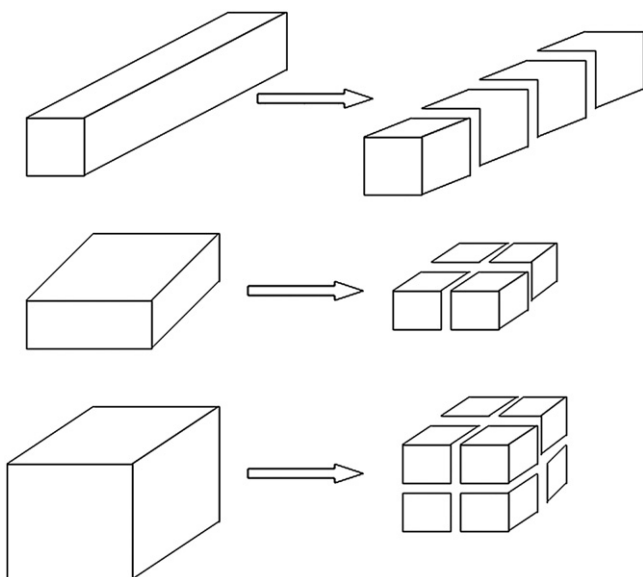


Fig. 3. Subdivision of a box.

4. A more generalized Downward Pass algorithm is designed. In the *Downward Pass*, the tree is traversed from the level 2 to leaves to compute the coefficients of local expansion. The local expansion associated with a box  $C$  is the sums of two parts. First, the L2L translation collects the coefficients of parent. Second, the M2L translation collects the coefficients of multipole expansion of the boxes which are the children of the neighbors of  $C$ 's parent but are not adjacent to  $C$ . In the *Downward Pass* based on the adaptive tree, the child boxes of a single parent box (Fig. 3(a)) are included in the interaction list. Thus the M2L translations can be used among the child boxes of a single parent box. However, the standard algorithm always treats the child boxes of a parent box as neighbors. This is no longer valid for the adaptive tree.

The detailed description about the differences can be obtained in Refs. [14,15]. The algorithms and procedures of standard FMM can be found in Reference [39]. In the adaptive FMBFM, the multipole and local moments associated with a box, which are calculated directly from Eqs. (7), (17) and (24) at each level are stored and reused to the full extent. The block diagonal preconditioner used in the GMRES is calculated once, and then stored for all iterations. These works lead to a lot of CPU time saving, and they can further improve the efficiency of the FMBFM.

In the FMBFM, the expansion parameter  $p$  is given in the following form:

$$p = kD + c_0 \log(kD + \pi) \quad (26)$$

$D$  is the diameter of the cell on which the expansions are calculated.  $c_0$  is a number that depends on the precision of the arithmetic.

To compute the value of physical variable on domain field points which are far away from the boundary, another similar binary tree data structure is adopted to accelerate the integration.

#### 5. Numerical examples

The adaptive FMBFM with quadratic discontinuous elements, which are defined either on quadrilateral or on triangular, has been implemented in a code written in C++ language and tested by four acoustic wave problems in this section. All the computations are carried out on the same desktop computer with an Intel(R) Dual-Core CPU (2.6 GHz) and 2 GB memory.

In all the numerical examples, the sound potential  $\phi$  we used is complex sound potential. The maximum number of the quadratic elements in leafs is 20. The multipole expansion terms  $p$  is evaluated through the following equation:

$$p = [kD + 5.0 \log(kD + \pi)] + 1, \quad (27)$$

where the  $[\bullet]$  denotes the integer part. In the GMRES solver, we stop the iteration when the relative error is less than  $10^{-3}$ .

To assess the accuracy of the adaptive FMBFM, we calculate the error of nodal values. And the error is defined as following form:

$$\text{error} = \frac{1}{|\phi|_{\max}} \sqrt{\frac{1}{m} \sum_{i=1}^m (\phi_i^a - \phi_i^r)^2}, \quad (28)$$

where  $m$  is the number of the nodes.  $\phi_i^a$  and  $\phi_i^r$  are analytical solution and numerical solution at node point  $i$ , respectively.  $|\phi|_{\max}$  is the maximum value among the analytical solutions.

##### 5.1. Validation of the adaptive FMBFM with high order element

A pulsating sphere (Fig. 4) is employed as the first numerical example to demonstrate validity of the adaptive FMBFM for

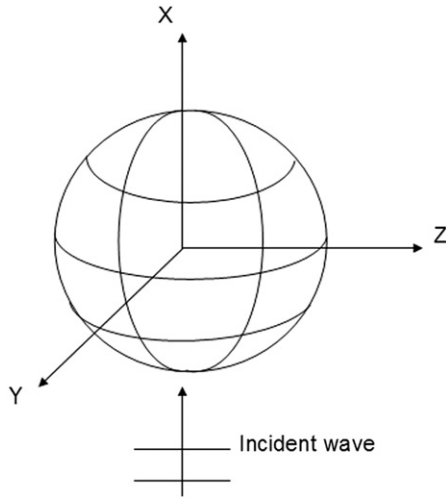


Fig. 4. A spherical body.

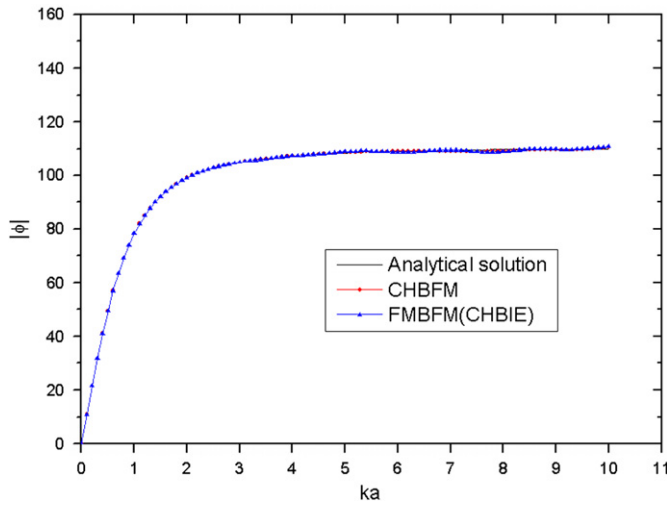


Fig. 5. Pressure at  $r=4a$  from the pulsating sphere.

radiation problems in an infinite acoustic domain. The radius of the pulsating sphere is  $a=1$ , and the boundary condition for the pulsating sphere is normal velocity  $v_0=1$  and  $\frac{\partial\phi}{\partial n}=ik\rho cv_0$  in another form. Where  $i=\sqrt{-1}$ ,  $\rho=1.29\text{ kg/m}^3$  and  $c=340.0\text{ m/s}$ . The whole spherical boundary surface is discretized into 80 discontinuous quadrilateral quadratic elements which contain in total 640 boundary nodes. For the radiation problem, the analytical solution to this problem is available and is described as:

$$\phi(r) = \frac{\rho cv_0(ika)a}{ika-1} \frac{1}{r} e^{ik(r-a)} \tag{29}$$

in which  $r$  stands for the distance between the ball center and the field point. The sound potentials for the nondimensionalized wave numbers  $ka$  ranging from 0 to 10.0 with 100 wave number steps at  $r=4a$  are shown in Fig. 5. From Fig. 5, we identified clearly that the results obtained by the adaptive FMBFM coincide well with the results obtained by CHBFM and the analytical solutions. It indicates that the truncation error introduced by the fast multipole expansion is very small for the radiation problems, and demonstrates that the adaptive FMBFM with quadratic elements is stable and accurate.

Furthermore, a rigid ball model (Fig. 4) is plotted to verify the adaptive FMBFM for scattering problems. As described before, the radius of the sphere is  $a=1$ , and centered at  $(0, 0, 0)$ . For the

scattering problems from a sphere with radius  $a$ , the analytic solution for the scattered potential at a distance  $r$  from the center of the sphere and at an angle  $\theta$  from the direction of the incoming wave is given by Ref. [40]:

$$\phi^s(r, \theta) = \sum_{m=0}^{\infty} -\frac{i^m(2m+1)j_m'(ka)}{h_m'(ka)} P_m(\cos \theta) h_m(kr) \tag{30}$$

where  $P_m$  is the Legendre function of the first kind.  $h_m$  denotes the spherical Hankel function of the first kind.  $j_m$  is the spherical Bessel function of the first kind. The formulation of the unit incident plane wave we used here is  $\phi^I=e^{-ikx}$ , and the rigid ball is meshed with 80 discontinuous quadrilateral quadratic elements (640 nodes). Fig. 6 shows the variation of sound potential  $\phi$  at a distance  $r=4a$ , which is plotted versus the polar angle  $\theta$ , when the nondimensionalized wave numbers  $ka$  is a characteristic wave number,  $ka=\pi$ , at which wave number the CBIE usually suffers from the non-uniqueness solution problem. From Fig. 6, we identify again that the results obtained by the adaptive FMBFM coincide with the results obtained by CHBFM and the analytical solutions. Moreover, it demonstrates that the non-uniqueness difficulty of acoustic problems at the characteristic frequency can be circumvented by the adaptive FMBFM with CHBIE.

### 5.2. Performance study of the adaptive FMBFM with higher element

In order to further study the performances of the adaptive FMBFM with higher elements, a pulsating box model (Fig. 7) with wave number  $ka=1.0$  is used for illustrating the accuracy of the adaptive FMBFM. The overall dimensions of the model are  $2 \times 10 \times 2$ . The pulsating box is formulated by prescribing the normal velocity on the box surface produced by a pulsating sphere of radius  $a=1$ . Thus the boundary condition prescribed on the box is given as:

$$q = \frac{\partial\phi(r)}{\partial n} \tag{31}$$

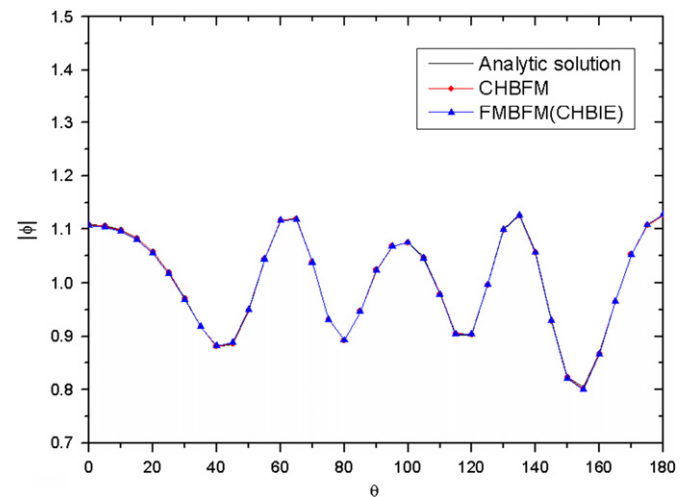


Fig. 6. Pressure at  $r=4a$  from the scattering sphere at the wave number  $ka=\pi$ .

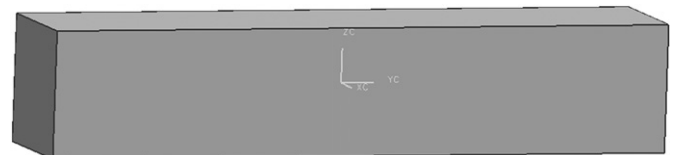


Fig. 7. A box model.

where  $\phi(r)$  is given in Eq. (29). This example is similar to one illustrated example in Ref. [40].

To perform a comparative study, the maximum number of the constant elements in leafs is set to be 80. We compare the relative errors of nodal values of sound pressure obtained by the FMBFM with constant elements and that of the FMBFM with quadratic elements are shown in Fig. 8. The comparative results showed that the results obtained by the adaptive FMBFM with quadratic elements (black line) are more accurate than that obtained by the adaptive FMBFM with constant elements (red line) when the number of nodes is more than 1400. The errors obtained by the adaptive FMBFM with quadratic elements decrease rapidly with the increasing number of the nodes.

Fig. 9 shows the computational total CPU time used to solve the pulsating box model. The total node numbers increase from 576 to 102,912. It can be seen from this figure that within the same number of nodes, the computation speed of the adaptive FMBFM with quadratic elements is of the same level with that of the adaptive FMBFM with constant elements. It can be concluded from Figs. 8 and 9 that the adaptive FMBFM with quadratic elements is more efficient than the adaptive FMBFM with constant elements for large-scale acoustic problems.

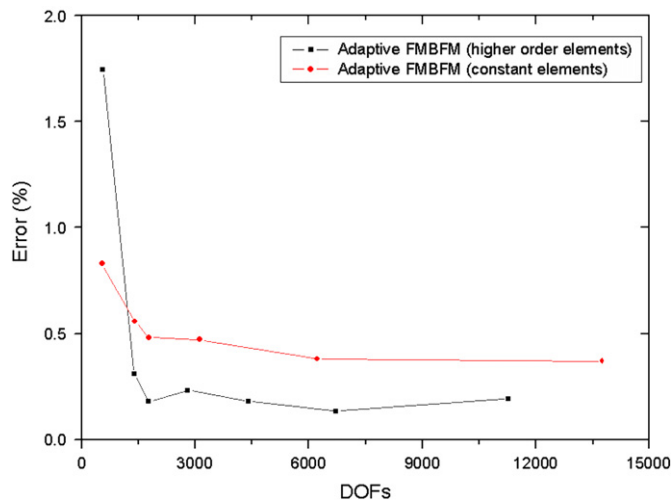


Fig. 8. The relative errors of nodal values for the pulsating box model. (For interpretation of the references to color in this figure legend, the reader is referred to the web version of this article.)

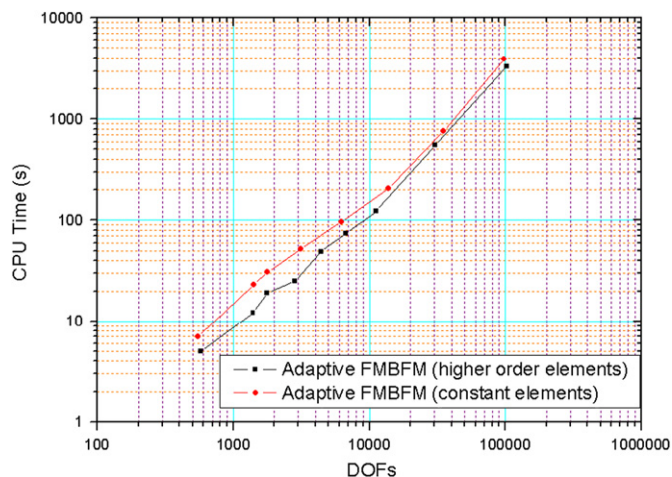


Fig. 9. The total CPU time used to solve the pulsating box model.

### 5.3. Performance study of the multipole expansion for far field evaluation

In this example, we study the efficiency of the multipole expansion for far field evaluation. A radiating sphere (Fig. 4) of radius  $a=1$ , centered at  $(0, 0, 0)$  with wave number  $ka=2.0$  is employed to test the accuracy and efficiency of the far field evaluation. The radiation problem on spherical is solved by the adaptive FMBFM with CHBIE. All the field points are distributed in a plane  $x=3.0$  with the dimensions  $[-5.0, 5.0] \times [0.0, 5.0]$  in  $y, z$  directions, respectively. The total number of the field points is 277. And we use  $p_0$  as the multipole expansion term for far field evaluation,  $p_0=p$ .

In this application, only the M2L translation is employed for the far field evaluation. The errors obtained by directly evaluation (BFM) and by the multipole expansion method (FMM) are plotted in Fig. 10 and the CPU time consumed by these two methods is illustrated in Fig. 11. In Figs. 10 and 11, the black line marked by BFM denotes the results evaluated by the conventional boundary face method and the red line marked by FMM denotes the results evaluated by the fast multipole expansion method.

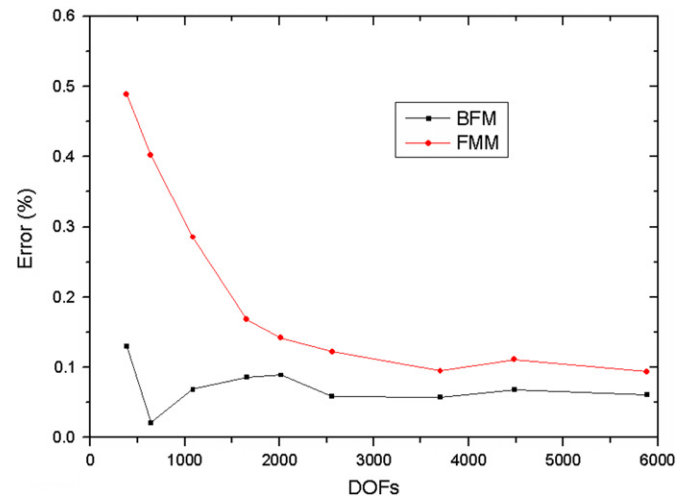


Fig. 10. The relative errors of the field points' values for far field evaluation.

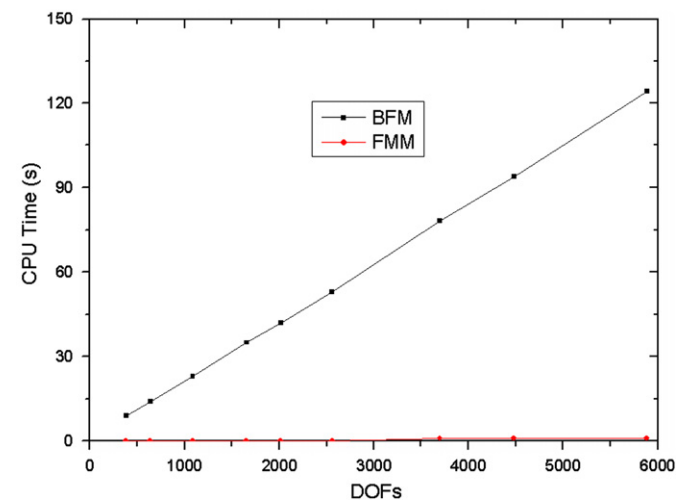


Fig. 11. The CPU time used for far field evaluation. (For interpretation of the references to color in this figure legend, the reader is referred to the web version of this article.)

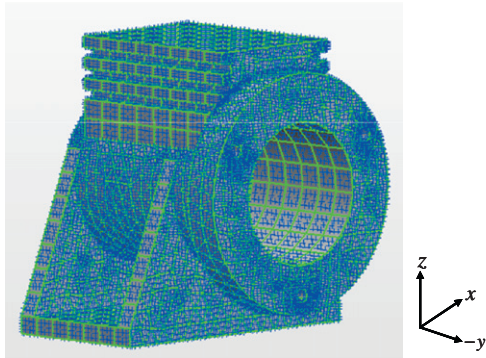


Fig. 12. A mechanical model meshed with 3554 elements.

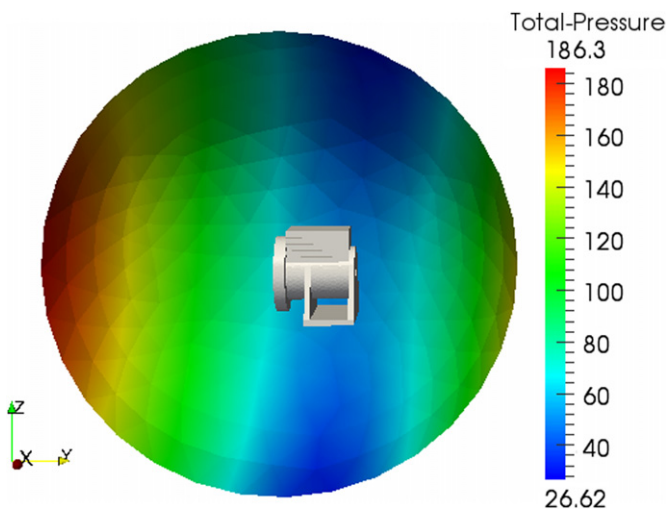


Fig. 13. The sound pressure for the mechanical model.

In Fig. 10, the error level obtained by FMM approaches that obtained by BFM with an increasing number of the node. The CPU time consumed by the FMM is much less than that by the BFM at the same number of nodes, which can be found in Fig. 11. This example illustrates that the FMM is a very efficient tool for accelerating the integration, and it is very suitable for the large-scale computation.

#### 5.4. A radiation problem on mechanical model

In the fourth example, the solution for the radiation problem on a relatively complicated mechanical model is presented to further demonstrate the applicability of the adaptive FMBFM for large-scale problem. The model is constructed with boundary representation (B-rep) data structure obtained from the commercial CAD software UG-NX 4.0, and it is shown in Fig. 12. The overall dimensions of the model are  $[-0.9, 0.9] \times [0, 1.575] \times [-0.926, 0.926]$  in  $x, y, z$  directions, respectively. The boundary condition for the model is a uniform normal velocity  $v_0 = 1.0$  on the model surface, and  $\frac{\partial \phi}{\partial n} = ik\rho c v_0$ . The wave number is  $k = 1.0$ . In total 3554 quadrilateral quadratic and triangular quadratic elements (22,700 nodes) are employed to discretize the model. The number of the field points in this example is 189. And all the field points locate on the sphere surface with radius equal to 5.0, center at  $(0, 0, 0)$ . The distribution of sound pressure on field points is shown in Fig. 13. The total CPU time used for this example is 931 s. It demonstrates that the integration of the adaptive FMBFM with the UG-NX is successful, and the presented FMBFM can solve the problems with complicated geometry.

## 6. Conclusions and future work

In this paper, an adaptive fast multipole boundary face method with quadratic elements based on the well-known Burton-Miller equation is presented to solve the radiation and scattering problems of exterior acoustic wave in 3-D. The results of the numerical examples demonstrate that the accuracy, efficiency and validity of the adaptive FMBFM for large-scale acoustic radiation and scattering problems. Comparison study showed that the FMBFM with quadratic elements out-performs the FMBFM with constant elements respect to accuracy and efficiency with employing the same number of the elements. In addition, the CAD models, even with complicated geometry, are directly converted into the FMBFM models. Thus the presented method provides a new way for automatic simulation.

The adaptive FMBFM is an extension of the adaptive tree for the fast multipole hybrid boundary node method (FM-HBNM) [14,15]. The FMBFM has been integrated into the widely used commercial CAD package UG-NX. Thus it is able to handle acoustic problems on complicated geometries. The application of quadratic elements further improves the computational accuracy and efficiency. The adaptive tree with tight bounds, which is constructed by a binary tree, is adopted in this paper. It uses rectangular boxes instead of cubes, and the boxes are splitted according to the shapes of the computational models in the process of constructing the tree. Thus the adaptive tree is more flexible in match the geometry of the computational model, especially for the slender and shell-like structures.

It is noted that the FMM used in this paper is the original FMM in [30]. The work for further improving the efficiency of the present FMBFM by incorporating the new FMM proposed by Rokhlin [23] with is ongoing. Moreover, a solution for problems on multi-domains is also ongoing.

## Acknowledgements

This work was supported by National Science Foundation of China under grant numbers 10972074 and 11172098.

## References

- [1] Zhang JM, Qin XY, Han X, Li GY. A boundary face method for potential problems in three dimensions. *Int J Numer Meth Eng* 2009;80:320–37.
- [2] Qin XY, Zhang JM, Li GY, Sheng XM, Song Q, Mu DH. An element implementation of the boundary face method for potential problems in three dimensions. *Eng Anal Bound Elem* 2010;34:934–43.
- [3] Gu JL, Zhang JM, Sheng XM, Li GY. B-spline approximation in boundary face method for three-dimensional linear elasticity. *Eng Anal Bound Elem* 2011;35:1159–67.
- [4] Zhou FL, Zhang JM, Sheng XM, Li GY. Shape variable radial basis function and its application in dual reciprocity boundary face method. *Eng Anal Bound Elem* 2011;35:244–52.
- [5] Gu JL, Zhang JM, Sheng XM, Li GY. Isogeometric analysis in BIE for 3-D potential problem. *Eng Anal Bound Elem* 2012;36:858–65.
- [6] Zhang JM. Theory and application of stress analysis on complete solids based on boundary face method. *Comput Aided Eng* 2010;19:05–10.
- [7] Zhou FL, Zhang JM, Sheng XM, Li GY. A dual reciprocity boundary face method for 3D non-homogeneous elasticity problems. *Eng Anal Bound Elem* 2012;36:1301–10.
- [8] Chen IL, Chen JT, Liang MT. Analytical study and numerical experiments for radiation and scattering problems using the CHIEF method. *J Sound Vib* 2001;248(5):809–28.
- [9] Schenck HA. Improved integral formulation for the acoustic radiation problem. *J Acoust Soc Am* 1968;44:41–58.
- [10] Burton AJ, Miller GF. The application of integral equation methods to numerical solution of some exterior boundary value problem. *Proc R Soc London A* 1971;323:201–10.
- [11] Liu YJ, Chen SH. A new form of the hyper-singular boundary integral equation for 3-D acoustics and its implementation with  $c_0$  boundary element. *Comput Methods Appl Mech Eng* 1999;173:375–86.

- [12] Chen JT, Chen KH, Chen CT. Adaptive boundary element method of time-harmonic exterior acoustics problems in two-dimension. *Comput Methods Appl Mech Eng* 2002;191:3331–45.
- [13] Chen JT, Lee YT, Lin YJ. Analysis of multiple-spheres radiation and scattering problems by using null-field integral equations. *Appl Acoust* 2010;71:690–700.
- [14] Zhang JM, Tanaka Masa. An effective tree data structure in fast multipole method. *Trans JASCOME* 2006;6:17–22.
- [15] Zhang JM, Tanaka Masa. Adaptive spatial decomposition in fast multipole method. *J Comput Phys* 2007;226:17–28.
- [16] Anderson RJ. Tree data structures for N-body simulation. *SIAM J Comput* 1999;28:1923–40.
- [17] Rokhlin V. Rapid solution of integral equations of classical potential theory. *J Comput Phys* 1985;60:187–207.
- [18] Greengard L, Rokhlin V. A fast algorithm for particles simulations. *J Comput Phys* 1987;73:325–48.
- [19] Saad Y, Schultz MH. GMRES: a generalized minimal residual algorithm for solving nonsymmetric linear systems. *SIAM J Sci Stat Comput* 1986;7:856–69.
- [20] Sonneveld P. CGS: a fast Lanczos-type solver for nonsymmetric linear systems. *SIAM J Sci Stat Comput* 1989;10:36–52.
- [21] Liu YJ. A new fast multipole boundary element method for solving large-scale two-dimensional elastostatic problems. *Int J Numer Methods Eng* 2006;65:863–81.
- [22] K Yoshida. Applications of Fast Multipole Method to Boundary Integral Equation Method. Ph.D. Dissertation, Department of Global Environment Engineering, Kyoto University, 2001.
- [23] Rokhlin V. Diagonal forms of translation operators for the Helmholtz equation in three dimensions. *Appl Comput Harmon Anal* 1993;1(1):82–93.
- [24] Zhang JM, Tanaka Masa, Endo M. The hybrid boundary node method accelerated by fast multipole method for 3-D potential problems. *Int J Num Meth Eng* 2005;63:660–80.
- [25] Greengard L, Rokhlin V. A new version of the fast multipole method for the Laplace equation in three dimensions. *Acta Numer* 1997;3:229–69.
- [26] K Yoshida. Applications of Fast Multipole Method to Boundary Integral Equation Method. Ph.D. Dissertation, Department of Global Environment Engineering, Kyoto University, 2001.
- [27] Zhang JM, Zhuang C, Qin XY, Li GY, Sheng XM. FMM-accelerated hybrid boundary node method for multi-domain problems. *Eng Anal Bound Elem* 2010;34:433–9.
- [28] Shen L, Liu YJ. An adaptive fast multipole boundary method for three-dimensional potential problems. *Comput Mech* 2007;39(6):681–91.
- [29] Chen JT, Chen KH. Applications of the dual integral formulation in conjunction with fast multipole method in large-scale problems for 2-D exterior acoustics. *Eng Anal Bound Elem* 2004;28(6):685–709.
- [30] Epton MA, Dembart B. Multipole translation theory for the three-dimensional Laplace and Helmholtz equations. *SIAM J Sci Comput* 1995;16(4):865–97.
- [31] Darve E. The fast multipole method I: error analysis and asymptotic complexity. *SIAM J Numer Anal* 2000;38:98–128.
- [32] Chew WC. Recurrence relations for three-dimensional scalar addition theorem. *J Electromagn Waves Appl* 1992;6:133–42.
- [33] Gumerov NA, Duraiswami R. Recursions for the computation of multipole translation and rotation coefficients for the 3-D Helmholtz equation. *SIAM J Sci Comput* 2003;25(4):1344–81.
- [34] Shen L, Liu YJ. An adaptive fast multipole boundary method for three-dimensional acoustic wave problems based on the Burton-Miller formulation. *Comput Mech* 2007;40:461–72.
- [35] Bapat MS, Liu YJ. A new adaptive algorithm for the fast multipole boundary element method. *CMES Comput Model Eng Sci* 2010;58(2):161–83.
- [36] Wu HJ, Liu YJ, Jiang WK. Analytical integration of the moments in the diagonal form fast multipole boundary element method for 3-D acoustic wave problems. *Eng Anal Bound Elem* 2012;36:248–54.
- [37] Li S, Huang Q. A fast multipole boundary element method based on the improved Burton-Miller formulation for three-dimensional acoustic problems. *Eng Anal Bound Elem* 2011;35:719–28.
- [38] Meyer WL, Bell WA, Zinn BT, Stallybrass MP. Boundary integral solutions of three dimensional acoustic radiation problems. *J Sound Vib* 1978;59(2):245–62.
- [39] Liu YJ. *Fast Multipole Boundary Element Method: Theory and Applications in Engineering*. Cambridge: Cambridge University Press; 2009.
- [40] Seybert AF, Soenarko B, Rizzo FJ, Shippy DJ. An advanced computational method for radiation and scattering of acoustic waves in three dimensions. *J Acoust Soc Am* 1985;77:362–8.